

Modeling Flow and Transport in Saturated Fractured Rock to Evaluate Site Characterization Needs

Christine Doughty and Kenzi Karasaki

Earth Sciences Division
E.O. Lawrence Berkeley National Laboratory

Abstract

Using regional geographic, geologic, hydrologic, geophysical, and meteorological data for the Tono area in Gifu, Japan, we develop an effective continuum model to simulate subsurface flow and transport in a 4 km by 6 km by 3 km thick fractured granite rock mass overlain by sedimentary layers. Individual fractures are not modeled explicitly. Rather, continuum permeability and porosity distributions are assigned stochastically, based on well-test data and fracture density measurements. Large-scale features such as lithologic layering and major fault zones are assigned deterministically. The model simulates the steady-state groundwater flow through the site, then streamline tracing analysis is used to calculate travel times to the model boundary from specified monitoring points that represent leakage from a hypothetical nuclear waste repository. Model results for the head distribution compare favorably with head profiles in several deep boreholes and the overall groundwater flow is consistent with regional water balance data. Predicted travel times range from 1 to 25 years. Several other research groups also developed models based on the same data set, and a key feature of the work is a comparison between different models' results to highlight which aspects of site characterization need to be improved in order to increase confidence in model predictions. Because a field investigation program is ongoing, model results can potentially have a significant impact on future characterization activities. The effective porosity of the fracture network is the least well-constrained parameter of our model, and a wide range in travel times obtained by the different research groups (1 to 1,000,000 years) can be attributed to orders of magnitude differences in the effective porosities used. This underscores the importance of improved porosity estimates as a key component of future site characterization.

1. INTRODUCTION

The Japan Nuclear Cycle Development Institute (JNC) has initiated a multi-national project to investigate the uncertainties involved in the prediction of flow and transport behavior of a fractured rock mass. In the initial stage of the project, the H-12 flow comparison, several research organizations conducted numerical simulations with the same starting information regarding tracer transport through a hypothetical fractured rock mass (Oyamada and Ikeda, 1999). The groups' results were compared to identify and quantify the uncertainties in the model predictions. The present stage of the project takes a similar approach, but considers a real field site, a 4 by 6 by 3 km region surrounding the MIU site in the Tono area of Gifu, Japan. The main results of the different groups' models are the predicted travel times from specified monitoring points to the model boundary. There are no comparable field data available to directly validate the models, so, as in the first stage, model uncertainty is assessed by comparing among results of different models.

We believe that this is potentially a very fruitful exercise. We do not believe, however, that there is much to gain in comparing how computer codes solve algebraic equations. A larger and often overlooked uncertainty lies in the development of the conceptual model. Another source of uncertainty that is tightly related to the development of the conceptual model lies in site characterization. The choice of field tests to be performed and how tests are designed, executed, and interpreted can have a strong effect on the resulting conceptual model, and ultimately on predictions made with the model. For example, in the H-12 flow comparison, data were provided in a form tailored for a discrete fracture

network model, making development of an effective continuum model cumbersome. In contrast, in the present stage data are presented in a more basic form, enabling a variety of conceptual models to be developed on equal footing. A major potential benefit of the present project is the chance for differences in model predictions to highlight aspects of site characterization that need to be improved in order to increase confidence in the model predictions, thus guiding the direction of ongoing site characterization activities.

In our conceptual model, a stochastic permeability distribution is used to represent fractured rock as an effective continuum. Individual fractures are not modeled explicitly. However, large-scale features such as fault zones, lithologic layering, natural boundaries, and surface topography are incorporated deterministically. We think the geometric data of individual fractures are useful, but we only regard them as “soft data.” The reasons are as follows: (1) It is virtually impossible to test individual fractures to measure and determine their transmissivity in the field. Therefore, the fracture transmissivity quoted in the literature is invariably inferred from borehole flow tests by making certain assumptions regarding the flow geometry. The measured value is likely to be the effective transmissivity of a collection of interconnected fractures at unknown distances and directions. (2) Fractures are in general neither planar, circular, nor square. (3) Variability of the hydraulic conductance (transmissivity) within a fracture is likely to be larger than the variability among fractures. (4) Correlation between the parameterized fracture geometry (e.g., fracture density and orientation) and the hydraulic properties of fractured rock mass may or may not exist.

Furthermore, even if accurate information on the flow and transport properties of individual fractures were available, there is only a limited spatial regime in which modeling individual fractures (a discrete fracture network model) is useful. At small scales or low fracture densities, the few individual fractures present may be modeled explicitly, but it is quite likely that there will be no connected fracture flow path across the model. At large scales and high fracture densities, the many fractures present are likely to be quite well-connected, and thus more efficiently represented as an effective continuum. For the present problem the model extent (4 by 6 by 3 km) is far greater than the typical measured fracture spacing (8 per meter). Thus, we chose to construct an effective continuum model to simulate the groundwater flow and tracer transport.

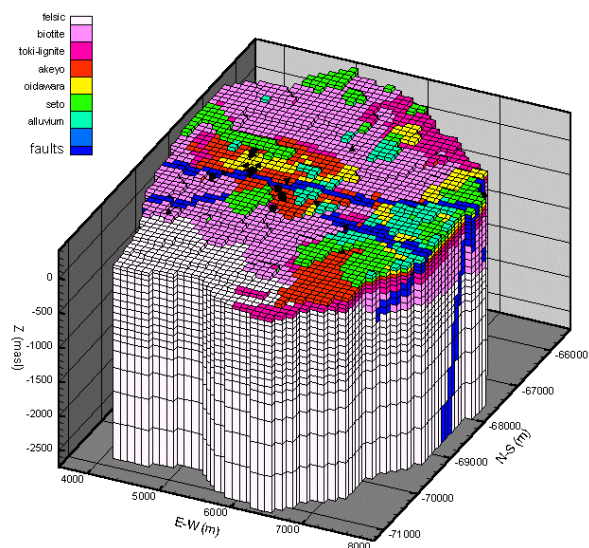


Figure 1. 3-D perspective view of the model used for the TOUGH2 simulations. Surface locations of wells are shown as black symbols.

2. METHODOLOGY

Simulator and streamtraces

The numerical simulator TOUGH2 (Pruess, 1987, 1991) is used for the flow calculations. For the present work, we employ a simplified equation of state module known as EOS9 (Wu et al., 1996) that considers only a single component (water) under isothermal conditions (20°C). The commercial graphics package Tecplot is used to determine groundwater travel times from the flow field calculated by TOUGH2. These travel times consider transport due to advection only; no diffusion or dispersion is included. Streamtraces originate from 24 specified monitoring points (four depths at each of six locations). A utility program takes the information recorded by Tecplot along each streamtrace (location, flow rate, velocity, permeability, and porosity) and calculates streamtrace length, travel time

to the model boundary, exit point on the boundary, and the mean and standard deviation of permeability and porosity along the streamtrace.

Available data and grid generation

We start with a regular 3D TOUGH2 grid of total extent 4.4 km by 5.9 km by 3.75 km. The basic grid block size is a 100 m by 100 m by 100 m cube. This size was chosen to be comparable to the typical length of the open interval during well tests. Grid block thickness decreases to 50 m between $z = 0$ masl and the top of the model at $z = 375$ masl, to enable better representation of surface topography changes. Grid block thickness gradually increases below $z = -1000$ masl since no data are available to constrain the model (the deepest well extends only to $z = -750$ masl) and flow variability is expected to be gradual at depth. Next, we trim the grid laterally to reproduce the irregular 4 by 6 km model boundary that follows natural topographic boundaries such as ridgelines and the Toki River. Then, we trim the grid vertically to match surface topography, as given by a 20 m by 20 m resolution digital topography map (dtm). We include the following features of interest deterministically by assigning grid blocks to different material types:

- The Tsukiyoshi fault is represented as a plane with location and orientation inferred from the surface trace, borehole occurrences, and seismic profiles. Several smaller surface lineaments identified from satellite or aerial images that are also identified in boreholes are modeled explicitly as well.
- Lithofacies changes observed in boreholes are kriged to form surfaces. These surfaces provide the boundaries between different material types in the model.
- The sediment/bedrock boundary inferred from an electrical resistivity survey is used as the boundary between the uppermost granite (Biotite) and the lowermost sedimentary rock (Toki-lignite bearing rock).

The resulting model is shown in Figure 1.

Property assignment

Each grid block represents an effective fractured continuum with permeability and porosity assigned stochastically based on field measurements. Permeability is proportional to hydraulic conductivity K , which is determined from slug tests and pumping tests conducted using packed-off intervals in boreholes. Because many of the intervals used for the tests are of the same order as the grid block size, we assume that there is no need to scale up or scale down K values measured during well tests, and that they directly represent effective continuum conductivities. Grid block conductivity values are drawn from random distributions for each material type. The distributions are constructed by resampling field measurements, unless there are not enough measurements for a given material type to make resampling viable, in which case a log-normal distribution is used. Table 1 summarizes the material types and conductivity distributions used for the model and Figure 2 illustrates the $\log_{10}K$ distributions that are constructed by resampling.

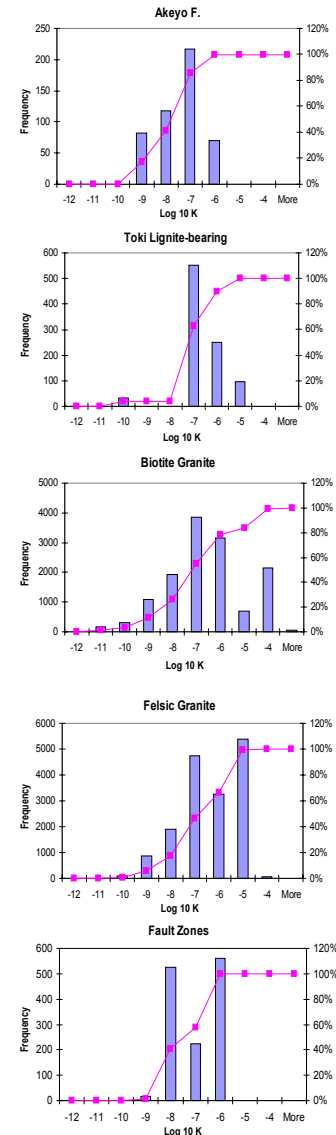


Figure 2. Distributions of $\log_{10}K$ obtained from slug tests and pumping tests. Each conductivity value is weighted by the length of test interval; frequency shows the number of grid blocks that are assigned a conductivity in the corresponding range.

Porosity ϕ is calculated as the product of fracture aperture w and fracture density d , with aperture determined from K and d using the cubic law:

$$\phi = w d = (12 K \mu / d)^{1/3} d = (12 K \mu d^2)^{1/3}. \quad (1)$$

Note that effective continuum conductivity K is related to the actual conductivity of an individual fracture K_f according to $K = K_f w d$. Fracture density measurements are sparse and there is no obvious correlation between fracture density and conductivity, so fracture density measurements from all lithological layers are combined to determine a mean fracture density of 7.95 m^{-1} and a standard deviation of 5 m^{-1} . For most of the lithological layers, fracture densities are drawn from a normal distribution with these moments, which is truncated at a small positive number (0.01 m^{-1}) to ensure that fracture density is always positive. However, for the Biotite and Felsic granites, fracture density distributions are created by resampling density measurements from that lithofacies.

For each grid block, after K and d have been drawn from the appropriate distribution, Equation (1) is applied to determine ϕ . The resulting model porosity statistics are summarized in Table 1. Note that ϕ must be positive, but that the standard deviation is typically the same magnitude as the mean, implying that the ϕ distribution arising from Equation (1) is distinctly non-normal.

Model porosity is considered to be less well constrained than model conductivity for several reasons. First, basing porosity estimates on fracture density measurements is problematic because a high percentage of observed fractures may not contribute to flow at all. Moreover, the cubic law can greatly misrepresent the relationship between fracture aperture and conductivity, and even if it is valid, the hydraulic aperture used in the cubic law tends to underestimate the volumetric aperture relevant for transport. Finally, there are few fracture density measurements available for materials other than the Biotite granite. Note that no data whatsoever are available for depths below 1000 m. Hence, all model properties there are quite uncertain.

Boundary conditions

- Surface topography guides us in determining the nature of the lateral boundary conditions for shallow portions of the model: the model is closed along ridgelines, whereas constant-head boundaries exist in a valley to the northeast (NE) and along the Toki River at the model's southern edge (Figure 3). However, it is unknown how deep these boundary conditions should be applied. It may be that at great depth, local surface topography has little or no effect on regional groundwater flow, and larger-scale, regional topographic trends determine appropriate boundary conditions. In the absence of any actual data, we assign the constant-head boundaries shown in Figure 3 over most of the model depth.

Table 1. Summary of material properties used in the model. For materials with no data available, use average for all materials

Material Type	Number of conductivity measurements	Log ₁₀ K (m/s)		Type of distribution used for log ₁₀ K	
		Mean	S.D.		
Alluvium	0	-7.9	1.6	Normal	
Seto group	0	-7.9	1.6	Normal	
Oidawara	1	-8.7	1.6	Normal	
Akeyo	11	-7.9	0.8	Resampled	
Toki lignite-bearing	21	-7.0	0.9	Resampled	
Biotite granite	192	-7.1	1.7	Resampled	
Felsic granite	46	-6.9	1.1	Resampled	
Faults	12	-7.7	1.0	Tsukiyoshi resampled; other faults normal	
Material Type	Number of fracture density measurements	Fracture density (m ⁻¹)		Model Porosity	
		Mean	S.D.	Mean	S.D.
Biotite granite	57	7.7	4.2	3.9E-4	5.9E-4
Felsic granite	4	10.8	4.2	3.5E-4	2.7E-4
Overall	67	7.9	5.0	3.2E-4	4.2E-4

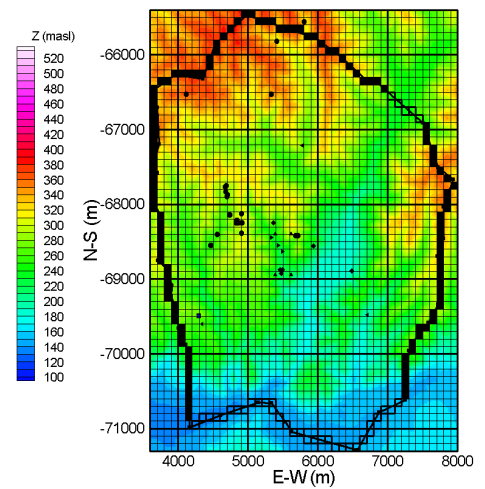


Figure 3. Plan view of the model's lateral boundary, superimposed on the digital topography map of the area. Closed boundaries are shown as filled-in black squares and constant-head boundaries are shown as open squares. Smaller black symbols identify wells.

- The bottom of the model is closed. In the three deepest layers of the model, below the depths of any field data, the permeability of the model gradually decreases. This is intended to reproduce a gradual closing of fractures due to the increase in lithostatic pressure with depth.
- The top of the model is held at a head value equal to the surface elevation, to represent a near-surface water table. Flow from the constant head boundary into the model represents subsurface recharge. This configuration eliminates the need to model percolation through the vadose zone, which is a highly non-linear process and hence computationally intensive.
- The Tono mine is represented as a mass sink at the sedimentary/bedrock interface, with a constant strength equivalent to $1500 \text{ m}^3/\text{month}$, determined by time-averaging outflow measurements at the mine.

3. RESULTS

Results of preliminary sensitivity studies that were used to choose the boundary conditions are described first, followed by results for our chosen base case, an alternative case with lower permeability in the Tsukiyoshi fault, and a subsequent sensitivity study on the boundaries representing rivers.

Preliminary boundary condition variations

In these sensitivity studies, permeability and porosity are uniform within each material type rather than being drawn from random distributions, to more clearly illustrate the effects of alternative boundary conditions.

Thickness of lateral constant-head boundaries

How deep to apply the constant-head boundaries is a major point of uncertainty. Figure 4a illustrates the effect of limiting the constant-head portion of the lateral boundaries to the 250 m just below the ground surface. The shape of the flow paths away from the monitoring points and the location at which they leave the model are much different than in Figure 4b, where nearly the entire height of the model is open. Careful thought is required in order to choose appropriate boundary conditions for a large model such as the present one, in which surface effects may or may not be significant at great depths.

Nature of closed lower boundary

It is often expected that permeability should decrease as depth increases, due to increasing lithostatic pressure that tends to close fractures, pore spaces, or other fluid flow paths. No such trend was observed in the well test data collected, but the model extends more than 2 km below the deepest well penetration. Figures 4a and 4b show flow paths for no permeability decrease with depth, but in Figure 4c, permeability in each of the bottom three layers decreases by a factor of three from the permeability above it. This gradual permeability decrease serves to limit fluid flow in the deepest portion of the model, making the lower no-flow boundary a gradational boundary rather than an abrupt one. If permeability does in fact decrease with depth, the choice of lateral flow boundary conditions at depth becomes less critical, as little fluid flow occurs there regardless of the boundary conditions applied.

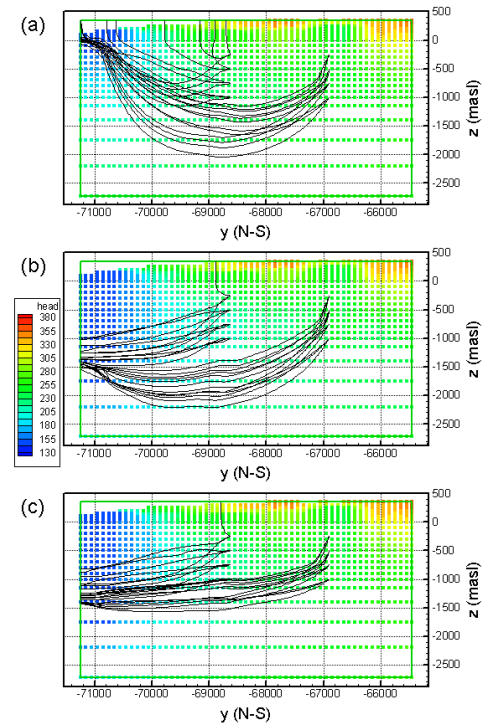


Figure 4. North-south cross-sectional (y-z) view of the streamtraces from the monitoring points. All x (E-W) values are projected on a single plane. In (a) the lateral constant-head boundaries extend less than 500 m below the ground surface; in (b) and (c) they extend over all but the lowest two layers of the model. In (c) the permeability in each of the lowest three layers is three times smaller than the permeability above it.

Multiple realizations of base case

Our base case includes the features shown in Figure 4c: lateral constant-head boundary conditions that extend over most of the model thickness and a gradual decrease in permeability at depth, because we believe these are reasonable choices. However, there is no direct evidence to support them, and as illustrated in Figure 4, they have important ramifications for fluid flow paths. The base case simulation was conducted for uniform permeability and porosity within each material type and for 10 realizations of random permeability and porosity distributions. Simplified water balances for each realization are presented in Table 2. The recharge quantity is about a factor of two smaller than the value inferred from rainfall, evaporation, and streamflow data. Most of the outflow is to or below the Toki River, but a small fraction leaves the model through a small low-elevation section to the northeast. Based on the topography of the surrounding area, this may not be reasonable, and is further investigated below. There is a marked difference between uniform and random permeability distributions, with significantly more water moving through the system for random permeability fields. We expect that if spatially correlated random fields were used, throughflow would be even larger.

Table 2. Simplified water balances for base case realizations. Quantities are in kg/s with surface recharge converted to mm/yr in parentheses.

Case	Surface recharge	Outflow at Tono mine	Outflow through NE boundary	Outflow through Toki River boundary
J74(non random)	39 (68)	0.57	3.4	35.5
J74R	57 (98)	0.57	4.4	52.2
J74S	60 (104)	0.57	3.5	56.7
J74T	56 (96)	0.57	3.8	51.7
J74U	61 (104)	0.57	7.2	53.4
J74V	59 (102)	0.57	4.0	55.3
J74W	61 (105)	0.57	9.8	50.9
J74X	62 (107)	0.57	8.7	53.2
J74Y	55 (95)	0.57	5.2	49.6
J74Z	59 (101)	0.57	4.0	54.8
J74A	58 (100)	0.57	2.7	55.2

Table 3 compares streamtrace information among all the different base case realizations. The variation between the different random realizations is relatively small, which is not surprising considering that the quantities being compared already represent average behavior over the different streamtraces of each realization.

Multiple realizations of low-permeability Tsukiyoshi fault case

Although conductivity values determined for fault zones do not appear to be significantly different than those for granitic rocks (see Table 1), observed head increases below the Tsukiyoshi fault suggest that it may act as a low-permeability barrier to flow. To test this hypothesis, we consider a case in which the permeability of grid blocks representing the Tsukiyoshi fault is decreased by a factor of ten. Water balances do not differ significantly from the base case.

Table 3. Average streamtrace information for all base case realizations.

Base Case Realizations	Log ₁₀ K	Porosity	Length (m)	Travel time (yr)	Velocity (m/yr)
J74 (non-random)	-6.93	3.5E-04	3292	11.4	289
J74R	-5.95	4.0E-04	2840	6.9	412
J74S	-5.92	4.4E-04	3148	7.2	435
J74T	-5.93	4.2E-04	3090	8	386
J74U	-5.88	4.3E-04	3150	8.5	371
J74V	-6.05	3.9E-04	3246	8	404
J74W	-5.98	4.0E-04	2703	5.8	467
J74X	-5.94	4.3E-04	3255	8.3	394
J74Y	-5.93	4.4E-04	2928	7.5	392
J74Z	-5.97	4.1E-04	2863	6.2	459
J74A	-5.88	4.5E-04	2948	8.1	364
Average over 10 random realizations	-5.94	4.2E-04	3017	7.5	408
Std dev.	0.05	1.9E-05	178	0.9	33

Figure 5 shows head profiles at the location of Well MIU-2 for some of the realizations of the above two cases. Although there is a great deal of variability between the different realizations, the effect of assigning lower permeability to the Tsukiyoshi fault results in an obvious increase in head below the fault depth. Figure 6 shows an example of the streamtraces leaving the monitoring points. The general flow pattern is similar for the two cases, but the effect of decreasing permeability in the Tsukiyoshi fault is apparent in the less direct paths; average travel time increases slightly, from 7 to 9 years.

Variation of head levels at boundaries representing rivers

We varied the head level of the NE constant-head boundary to study its effect on both the local flow paths in that region and the overall water balance. Table 4 summarizes the water

balances for the cases considered and Figure 7 shows some of the streamtraces. Based on the larger-scale topography, we believe that the cases in which there is inflow to the model rather than outflow from the model through the NE boundary are more reasonable. Assuming a 10 m head increase at the boundary is equivalent to assuming that the water table at the boundary is quite near the ground surface, whereas throughout the rest of the model the water table depth averages 10 m. Borehole measurements throughout the area suggest that an average water-table depth of 10 m is reasonable and the presence of a river intersecting the open NE boundary makes a shallower water table there plausible. It is possible that assigning a similar increase in head at the Toki River boundary along the southern edge of the model may also be appropriate. As shown in Table 4, this change has a strong effect on the overall water balance. Further investigation of the local topography around the NE model boundary and the Toki River model boundary is needed to determine how best to assign river boundary conditions.

4. CONCLUSIONS

We have used a variety of surface and subsurface data to build a hydrologic flow and transport model of the 4 by 6 km region surrounding the MIU site. No one type of data provides enough information by itself, but each contributes to the overall effort. Table 5 summarizes how different data have been used so far, and proposes some potential future uses.

Model results suggest that the average travel time from the monitoring points to the model boundary is relatively short: about 7 years for the base case and about 9 years for the low-permeability Tsukiyoshi fault case. Decreasing the permeability in the Tsukiyoshi fault causes noticeable changes in the pressure profile near the fault, but not a wholesale change in flow pattern through the model.

For each case, there is significant variability among the different stochastic realizations in terms of the details of the streamtrace patterns, including model exit locations. However, if only average results such as the mean travel time or mean path length are considered, then variability among realizations is relatively small. Greater variability arises from imposing different boundary conditions or assigning low permeabilities to the Tsukiyoshi fault and deep model layers, emphasizing the need to establish a sound basis for determining these model properties. Another highly uncertain model parameter is the effective porosity, to which travel time estimates are very sensitive. The following subsections describe areas where further work would help reduce uncertainty in model predictions.

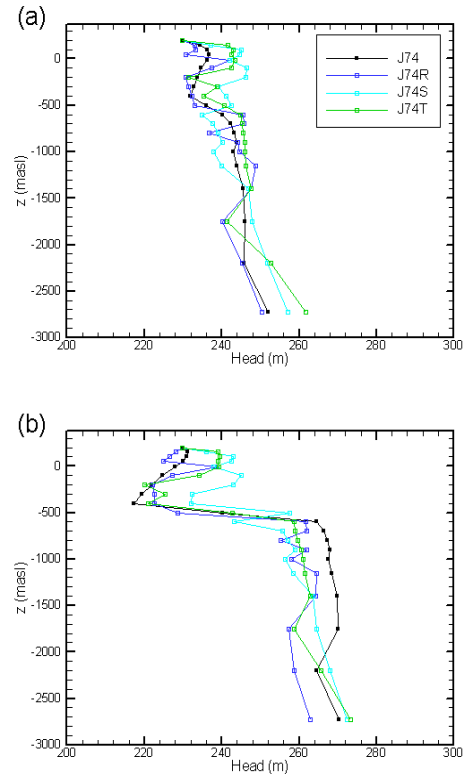


Figure 5. Head profiles at the location of Well MIU-2 for (a) the base case; and (b) the low-permeability Tsukiyoshi fault case. Cases J74R, J74S, and J74T represent different realizations of a random property distribution; Case J74 has uniform properties within each material type.

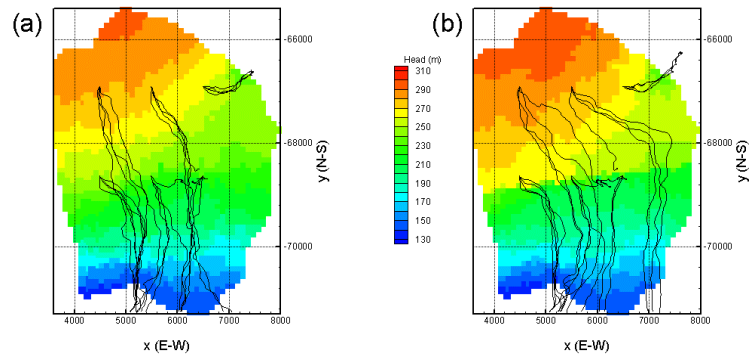


Figure 6. Streamtraces and head distributions for (a) the base case and (b) the low-permeability Tsukiyoshi fault case. The 3D streamtraces are projected to the model top surface. The head distribution is for $z = -1000$ masl.

Additional data needed

To better characterize the regional water balance, in particular the role of the shallow sedimentary layers in connecting surface infiltration and the underlying granitic basement, the following data would be useful:

- The hydrologic character of the sedimentary layers (i.e., is flow fracture-dominated?); conductivity and porosity values for shallow layers.
- Recharge estimates over a wider area (quantitative or qualitative information)
- The Toki River gain or loss over the model boundary
- Data on the river at the NE constant-head model boundary
- Other big contributors to the regional water balance (e.g., golf course irrigation)

Table 4. Simplified water balances for cases with different head values at lateral open boundaries. Quantities are in kg/s with surface recharge converted to mm/yr shown in parentheses.

Case	Surface recharge	Outflow at Tono mine	Outflow through NE boundary	Outflow through Toki River boundary
Base case (J74R)	57 (98)	0.57	4.4	52.2
Add 5 m to head at NE boundary	55 (94)	0.57	2.2	52.3
Add 10 m to head at NE boundary	52 (90)	0.57	-0.2	52.4
Add 15 m to head at NE boundary	50 (86)	0.57	-2.8	52.5
Add 10 m to head at NE and Toki River boundaries	30 (51)	0.57	-0.02	29.6

Possible additional site characterization

To better quantify the permeability and porosity distributions used in the model, the following site characterizations activities would be valuable:

- Isotope or other naturally occurring tracers (to estimate residence or travel times between various regions, to get a better understanding of regional groundwater flow)
- Active tracer tests (to help constrain the estimation of fracture porosity)
- Longer-term pumping tests (most of conductivity information comes from slug tests, which may be less reliable than pumping tests)
- Cross-hole well tests (to develop a better understanding of fracture connectivity)

ACKNOWLEDGMENTS

This work was supported by Japan Nuclear Fuel Cycle Corporation (JNC) and Taisei Corporation of Japan, through the U.S. Department of Energy Contract No. DE-AC03-76SF00098. We

are particularly indebted to Mr. Atsushi Sawada of JNC and Mr. Yuji Ijiri of Taisei Corp. for useful discussions. We would also like to thank Mr. Shinji

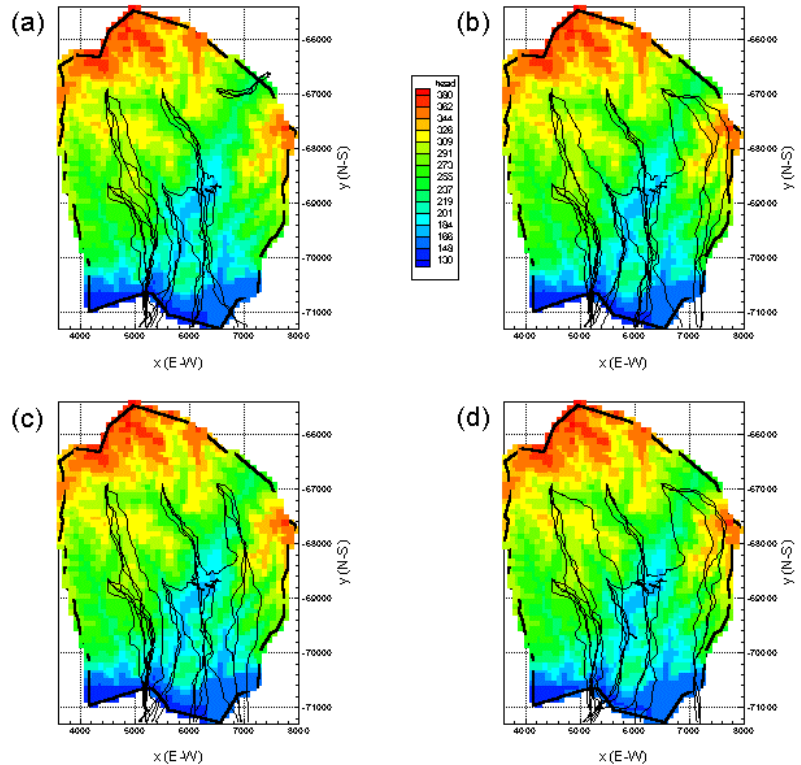


Figure 7. Plan view of streamtraces for a realization of the base case (J74R) with different head boundary conditions at the open boundaries: (a) the original head boundary condition; (b) a head increase of 10 m at the NE boundary; and (c) a head increase of 15 m at the NE boundary; and (d) a head increase of 10 m at the NE boundary and at the Toki River boundary.

Takeuci and Mr. Hiromitsu Saegusa for making various field data available to us. The authors would like to thank Dr. Stefan Finsterle for his critical review.

REFERENCES

Oyamada, K. and T. Ikeda, Uncertainty analysis on hydrologic modeling in heterogeneous media (CORE Collaborative Study), Japan Nuclear Fuel Cycle Development Institute TJ1400 99-023, 1999.

Pruess, K., TOUGH user's guide, Rep. LBL-20700, Lawrence Berkeley Laboratory, Berkeley, CA, 1987.

Pruess, K., TOUGH2 – A general-purpose numerical simulator for multiphase fluid and heat flow, Rep. LBL-29400, Lawrence Berkeley Laboratory, Berkeley, CA, 1991.

Wu, Y.S., C.F. Ahlers, P. Fraser, A. Simmons and K. Pruess, Software qualification of selected TOUGH2 modules, Rep. LBNL-39490, Lawrence Berkeley National Laboratory, Berkeley, CA, 1996.

Table 5. Summary of data used to develop the 4x6 km model.

Data Type	Actual Use	Potential Use
Landsat images	Qualitative understanding of regional surface topography	Improve lateral model boundaries at great depths
Surface topography	Provide detailed topography that impacts shallow groundwater flow	
Seismic profiles	Locate faults in 2-D sections	
Electrical resistance	Provide spatially extensive image of the sediment/bedrock boundary	
Surface geological map	Verify granite outcrop locations in model	Improve assignment of shallow material types, especially among sedimentary rocks
Water balance data	Estimate average surface recharge into the model	Identify locations of especially large or small recharge
Wellbore lithologies	Assign material types	
Wellbore fracture identification	Determine stochastic distribution of fracture density for use in calculation of model porosity	
Well tests	Provide distributions of conductivity values for model	Use in inversion to determine conductivity of specific regions
Multi-packer monitoring	Investigate connectivity and flow barriers	Same as well tests
Drillers' notes		Identify high flow zones
Flow and temperature logs		Investigate regional groundwater flow